Journal of
Engineering Sciences
Faculty of Engineering
Assiut University
JES
مجلة
العلوم الهندسية
كلية الهندسة
جامعة أسيوط
journal homepage: http://jesaun.journals.ekb.eg

Proposed Shear Design Method for Continuous Reinforced Concrete Beams Considering Moment Redistribution

Received 19 April 2025; Revised 31 August 2025; Accepted 31August 2025

Tarek Abdelaleem [1]
Mohamed Zakaria [2]
Hesham M. A. Diab [3]
Yehia. A. Hassanean[4]

Keywords
Shear strength, web reinforcement ratio, Moment redistribution, Proposed equation, Continuous beams, Finite element modelling.

Abstract: Current shear design provisions for continuous reinforced concrete (RC) beams inadequately account for the coupled effects of shear span-to-depth ratio (a/d) and moment redistribution, often leading to conservative or unsafe predictions. This study addresses this gap through an integrated approach combining nonlinear finite element modelling and full-scale laboratory testing. Eleven continuous beam models with varying (a/d) ratios and transverse reinforcement percentages were analysed using ANSYS, and three full-scale RC beams were tested under symmetrical four-point loading. Results show that reducing (a/d) increases shear strength by up to 42% but reduces redistribution capacity, while changes in transverse reinforcement ratio have negligible influence on redistribution. A new empirical equation is proposed to predict moment redistribution ratios, incorporating a/d effects, with prediction errors within ±5% of experimental and numerical results. Compared with current code expressions, the proposed model offers consistently higher accuracy across a wide range of geometries. The findings provide a unified framework linking shear capacity and redistribution limits, enabling more rational and reliable shear design provisions for continuous RC beams in major structural codes.

1. Introduction

Shear failure in reinforced concrete (RC) beams is typically sudden and brittle and once initiated it can lead to rapid structural collapse. For this reason, an accurate estimation of shear capacity is critical to ensuring ductility, serviceability, and overall safety throughout a structure's lifespan [1–4]. Insufficient shear resistance can cause wide diagonal cracking, premature stiffness loss, and early degradation. Despite this importance, many experimental data and code provisions have been developed for simply supported beams [5,6], which do not replicate the stress reversals and interaction effects present in continuous members.

[1] Assistant Professor, Civil Engineering Department, Assiut University, Egypt. Tarekabdelaleem@aun.edu.eg
[2] Assistant Lecturer, Faculty of Engineering, Sohag University, Egypt. m_zakaria@eng.sohag.edu.eg
[3] Professor, Civil Engineering Department, Faculty of Engineering, Assiut University, Egypt. diab@aun.edu.eg
[4] Professor, Civil Engineering Department, Faculty of Engineering, Assiut University, Egypt. yehia.mekhaimer@eng.au.edu.eg

https://doi.org/10.21608/JESAUN.2025.376890.1483

Continuous RC beams, being statically indeterminate, experience moment reversal near supports, inelastic regions under high load, and combined flexural–shear action [7,8]. Several experimental studies have shown that continuity can increase shear capacity by 30–50% relative to predictions based on simply supported beam formulas [9,10]. This improvement has been attributed to multiple mechanisms, including redistribution of internal forces [9,11], additional axial compression in the web [12,13], enhanced dowel action from longitudinal reinforcement [14,15], and smaller crack widths improving aggregate interlock [10,16].
Nevertheless, major design codes such as ACI 318-19 [17], BS 8110 [18], and Eurocode 2 [19] still use shear expressions largely derived from simple-span beam testing. While some adjustments for continuous members exist — for example, modified stirrup requirements or alternative definitions of shear span — there is no comprehensive framework that quantifies the full influence of continuity on shear capacity. An additional factor often overlooked in continuous beam design is the ability of the structure to redistribute moments through plastic hinge formation near supports [7,21–23]. The extent of redistribution, typically expressed as the moment redistribution ratio $\boldsymbol{\beta}$, is a key indicator of ductility and the ability to shift internal forces under ultimate loads.

$$\boldsymbol{\beta = \frac{M_e - M_{ex}}{M_e} x100} \quad (1)$$

In continuous beam analysis, the experimental bending moment at any stage is denoted as $\boldsymbol{M_{ex}}$, while $\boldsymbol{M_e}$ refers to the corresponding values at midspan and central support obtained from elastic theory. Although several models predict the moment redistribution ratio, β [7], they rarely account for the influence of the shear span-to-depth ratio (a/d), which plays a decisive role in redistribution potential [24–26]. For example, the expression by A. Tarek et al. [7] relates β to the quantities of tensile reinforcement in positive (A_{ss}) and negative (A_{sh}) moment zones, incorporating the steel ratio (ρ_s) and its minimum required value (ρ_{smin}). However, it does not consider the effect of a/d. Lower a/d ratios often reduce ductility, thereby limiting the extent of redistribution achievable in practice.

$$\boldsymbol{\beta = 32.763 \ln \frac{A_{ss}}{A_{sh}} + 5.0611 \ln(\rho_s - \rho_{smin}) + 13.6988} \quad (2)$$

The interaction between shear strength and redistribution is a defining feature of continuous RC members. Lower a/d values, associated with deeper sections, typically enhance shear capacity but restrict redistribution, whereas higher a/d ratios can permit substantial redistribution but increase vulnerability to premature shear failure if not adequately reinforced [24–26].
This study addresses the gap by examining how a/d influences both shear behavior and redistribution capacity in continuous RC beams. The approach combines nonlinear finite element simulations, new analytical formulations, and full-scale testing. The proposed shear capacity model is validated against experimental results from the present work and a wide range of published data, including tests on members reinforced with fiber-reinforced polymer (FRP) bars. Based on these results, guidelines for setting safe redistribution limits are proposed. The results contribute to a better understanding of shear behavior in continuous RC

beams—critical elements in buildings, bridges, and structural frames—and support the development of design provisions for FRP-reinforced members, which differ in shear transfer and deformation characteristics from conventional steel-reinforced systems.

2. Experimental program

2.1. Specimens Details

To evaluate the effect of shear span-to-depth ratio (a/d) on the shear behavior and moment redistribution of continuous reinforced concrete beams, three two-span specimens were designed, constructed, and tested. The primary variable was the (a/d) ratio, while all other geometric and reinforcement parameters were kept constant. Each beam measured 4000 mm in overall length, comprising two equal spans of 1900 mm. The cross-section was rectangular, 200 mm in width and 300 mm in total depth, with an effective depth of 270 mm. The beams were loaded using a symmetrical four-point bending configuration, applying a single concentrated load at the center of each span. The shear spans were set to 700 mm, 550 mm, and 400 mm, corresponding to a/d ratios of 2.6, 2.0, and 1.5, respectively. All specimens were proportioned to fail in shear prior to reaching their flexural capacity. To suppress flexural failure, the longitudinal reinforcement layout included three high-yield 16 mm diameter bars placed in the top layer over the central support and four 16 mm diameter bars at the bottom in the midspan regions. Shear reinforcement consisted of 6 mm mild steel stirrups spaced at 200 mm center-to-center within the shear-critical zones and 8 mm stirrups spaced at 100 mm in the external shear spans. To enhance anchorage and prevent splitting failures, the longitudinal bars were bent at the ends, providing a development length equal to the effective depth. A schematic representation of the reinforcement arrangement and beam geometry is provided in Table 1 and Figure 1.

2.2. Material Characteristics

All beams were produced using ready-mix concrete designed for a nominal compressive strength of 25 MPa, with a maximum aggregate size of 20 mm. To verify the actual strength of each batch, four 150 mm cubes were cast alongside the beams and cured under identical conditions. Compressive testing was performed on the same day as beam loading, and the average strength of the four cubes was adopted as the representative concrete strength for that batch. For longitudinal reinforcement, 16 mm high-yield deformed bars were employed at both the tension and compression zones. The transverse reinforcement in the shear-critical regions consisted of mild steel stirrups with diameters of 6 mm and 8 mm. The mechanical properties of all reinforcing bars were established through standard tensile testing, providing values of yield strength, ultimate strength, and modulus of elasticity that were directly incorporated into the analytical and numerical models. A complete summary of these properties is presented in Table 2.

2.3. Test Setup and Procedure

Each specimen was arranged as a two-span continuous beam resting on three steel supports. The middle support functioned as a pinned connection, restraining horizontal movement but

permitting rotation, while the end supports were modeled as rollers, allowing longitudinal displacement. This ensured that the intended boundary conditions were reproduced accurately. Loading was applied using a 5000 kN EMS hydraulic testing frame. A rigid steel spreader beam transferred the actuator force into two equal concentrated loads, symmetrically placed within each span. The reaction at the central support and the total applied load were measured through calibrated load cells to ensure accuracy of the applied forces. To capture the deformation response, linear variable differential transformers (LVDTs) with high sensitivity were positioned at midspan and other critical points along the beam. Longitudinal reinforcement strains were monitored using electrical resistance strain gauges fixed at the tension reinforcement in both the midspan and central support regions. Additional strain gauges were bonded to the concrete compression zone (see Figure 3) and to selected internal stirrups in the shear-critical regions to record shear strains in the transverse reinforcement. Crack propagation was tracked using a precision LVDT (0.001 mm accuracy) mounted across major cracks to measure incremental crack widths throughout the loading sequence. All instruments were connected to a data acquisition system, enabling continuous recording of load, deflection, reinforcement strain, and crack width from the initial elastic stage up to ultimate failure. The reinforcement layout and overall experimental setup are illustrated in Figures 1 and 2, while detailed material and specimen properties are summarized in Table 2.

Table 1: Compressive strength of the tested beams and reinforcing configuration.

Beam	(f_c) (MPa)	$(\frac{a}{d})$	Longitudinal reinforcement		Flexural reinforcement ratio (%)	
			Top RFT	Bottom RFT	Top RFT	Bottom RFT
BS1	25	2.6	3 Φ16	4 Φ16	1.12	1.5
BS2	24	2				
BS3	24.5	1.5				

Table 2: Mechanical properties of steel reinforcement

Bar Type	Diameter (mm)	Nominal area (mm^2)	Yield strength (MPa)	Ultimate strength (MPa)	Modulus of Elasticity (GPa)
Steel bars	16	200	500	650	198
Steel stirrups	8	50	380	500	201
	6	28	360	450	198

2.4. Calculation of Moments and Redistribution

In the experimental program, internal moments were calculated using basic static equilibrium. Load cells at the steel beam (Fig.2) and supports recorded reaction forces. The sagging moment at mid-span and hogging moment at the central support were calculated using:

$$\boldsymbol{M_{sag.} = R.(\frac{l}{2} - a)} \quad \textbf{(3)}$$

$$\boldsymbol{M_{hog.} = R.\left(\frac{l}{2}\right) - \frac{p}{2} * a} \quad \textbf{(4)}$$

where R is the end support reaction, a is the shear span, and p is the total machine load.

For linear elastic moment values, standard beam theory was used assuming fully elastic behaviour. The moment redistribution ratio, β, was then determined as:

$$\boldsymbol{\beta = \frac{M_e - M_{ex.}}{M_e} * 100} \quad \textbf{(5)}$$

where $M_{ex.}$ is the experimentally determined moment at a given section and M_e is the corresponding elastic moment.

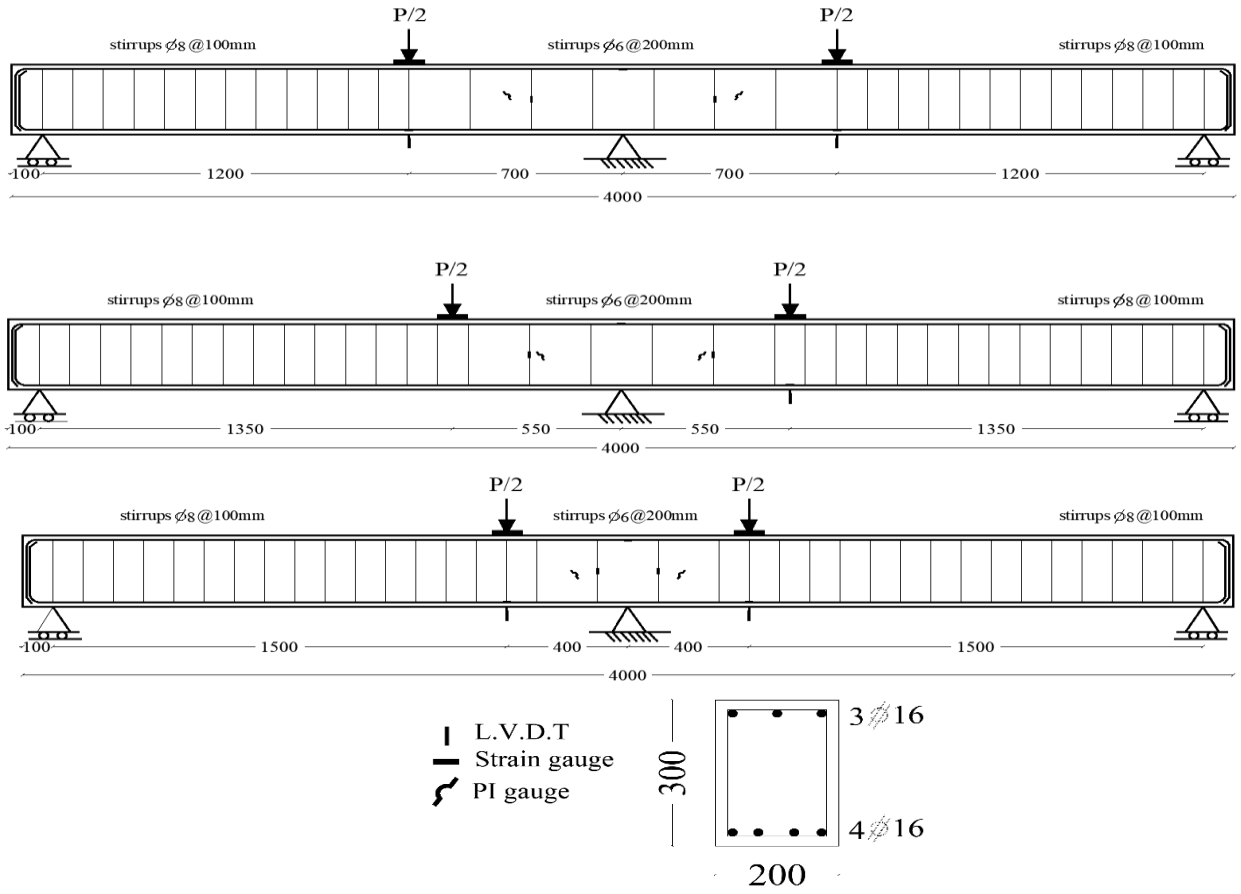

Fig. 1: Details of reinforcement of tested beams, typical cross-section.

Fig. 2: External instruments and a typical test setup.

3. Test results and discussion

3.1. Typical behavior and mode of failure

All three test beams, BS1, BS2, and BS3, exhibited similar cracking behavior and progression of damage leading to ultimate shear failure. The Initial cracks appeared as minor vertical flexural cracks in the hogging moment region near the middle support due to tension in the concrete. As loading was increased incrementally, wider diagonal shear cracks began to propagate from near the middle support towards the applied point loads. In beam BS1 with a shear span-to-depth ratio ($\boldsymbol{a/d}$) of 2.6, initial diagonal cracking was observed at an applied load of around 120 kN. The critical diagonal shear crack that resulted in failure initiated closer to the middle support and propagated towards the location of the load application as the load reached 190 kN. BS1 experienced a brittle and sudden shear failure crack through the mid-depth along one shear span. Beams BS2 and BS3, with lower $\boldsymbol{a/d}$ ratios of 2.0 and 1.5, respectively, were intentionally designed to fail in shear before reaching flexural capacity. Much like in BS1, diagonal shear cracks started to form and widen starting from the middle support as the applied loads gradually increased. For BS2 with $\boldsymbol{a/d}$ = 2.0, shear cracking progressed more extensively compared to BS1, leading to an ultimate shear failure crack and collapse at 223 kN. Beam BS3 exhibited substantial web shear cracking early on and failed suddenly at 270 kN along one shear span close to the middle support. The formation of additional bending cracks was restrained near the failure loads for beams BS2 and BS3. Overall, while all three test beams showed analogous cracking behavior, the shear cracks were more widely spread for lower $\boldsymbol{a/d}$ ratios. For every continuous beam that was tested, brittle diagonal tension cracking that started close to the middle support in a single shear span was the most common mechanism of failure, emphasizing the impact of severe shear. Figure 3 illustrates the crack propagation in beams BS1, BS2, and BS3, leading to a critical shear crack at failure.

Fig. 3: Cracking patterns and failure modes for test beams BS1, BS2, and BS3, showing diagonal shear failure initiating near the middle support.

3.2. Load deflection response

The relationship between applied load and corresponding midspan deflection was monitored for all test beams. The load-deflection behavior exhibited two distinct stages: an initial uncracking response followed by a post-cracking response after concrete cracking. In the pre-cracking stage, the load-deflection relationship was approximately linear with very little deviation. The stiffness was governed by the intact elastic modulus of the uncracked concrete in terms of compression and tension. After the formation of the first cracks due to the tensile cracking of concrete, the response transitioned to the post-cracking phase. With increasing applied loads, the stiffness degraded progressively as more extensive cracking occurred. The post-cracking stiffness and deflection depend on the axial stiffness of the reinforcing steel bars. All three test beams, BS1, BS2, and BS3, reached peak deflections of around 8-12 mm at failure, albeit at varying ultimate loads of 190 kN, 223 kN, and 270 kN, respectively. Beam BS1 with the highest $\mathbf{a/d}$ ratio of 2.6 exhibited the lowest stiffness throughout loading compared to BS2 and BS3, resulting in larger deflections. This demonstrates that reducing the shear span for constant depth decreases midspan deflections. The load-deflection plot for BS3 showed a plateauing behavior near peak load, indicating greater deformability before failure. In summary, with higher $\mathbf{a/d}$ ratios, initial cracking occurred at lower loads, and post-cracking stiffness as well as ultimate loads were reduced. However, deflections increased for larger $\mathbf{a/d}$ values at a given load. The experimental load-deflection plots validate that the shear span-to-depth ratio substantially influences the stiffness, strength, and ductility of continuous concrete beams. Similar observation was recorded by Mahmoud, [27] for ordinary RC beams with varying $\mathbf{a/d}$ ratios. Figure 4 shows the full load-deflection response across pre- and post-cracking regimes up to peak loads for all test beams. Table 3 shows the values of the deflection for all tested beams at cracking, yield, ultimate and failure load.

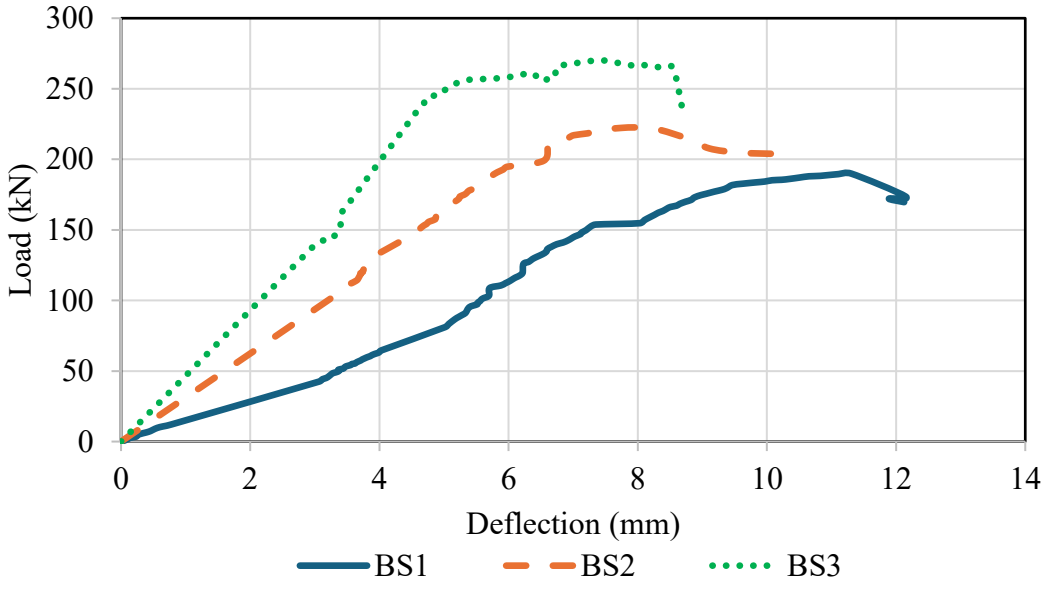

Fig. 4: Load–deflection responses of beams BS1, BS2, and BS3, illustrating the influence of shear span-to-depth ratio on stiffness and ductility.

Table 3: Deflection of the tested beams at different levels of loading.

Beam	At cracking load (mm)	At yield load (mm)	At ultimate load (mm)	At failure load (mm)
BS1	3.07	7.35	11.31	12.15
BS2	3.51	5.98	7.93	8.11
BS3	3.82	5.35	7.49	8.55

3.3. Shear strength

The ultimate shear loads, corresponding midspan deflections, bending moments, moment redistribution ratios, and failure modes observed from the three RC continuous beam tests are summarized in Table 4. The experimental results validate that the shear strength capacity of continuous RC beams is significantly affected by the shear span to depth ratio ($\mathbf{a/d}$). As the $\mathbf{a/d}$ ratio decreased from 2.6 to 2.0 for BS1 and BS2, the ultimate shear load increased by around 17% from 190 kN to 223 kN. Further reducing the a/d ratio to 1.5 for BS3 led to a 42% improvement in shear strength to 270 kN compared to BS1. Thus, substantially decreasing the shear span for a constant member depth considerably enhances the ultimate shear resistance. The extent of moment redistribution occurring between critical sections was also found to be influenced by the $\mathbf{a/d}$ ratio. Beams BS2 and BS3 with lower $\mathbf{a/d}$ values demonstrated increased moment redistribution capacity compared to BS1 with the highest tested a/d. This indicates that the degree of internal force transfer from sagging to hogging regions is higher for stockier members. However, BS3 with the minimum $\mathbf{a/d}$ exhibited lower ductility with more brittle, shear-dominated behavior. Thus, while lower shear spans allow greater moment redistribution, excessively short spans can result in sudden shear failures after yielding. In summary, reducing the shear span to depth ratio enhances both the ultimate shear strength as well as the moment redistribution capacity prior to failure. But decreasing $\mathbf{a/d}$ beyond an optimum level led to abrupt shear failure at elevated loads without prior flexural yielding.

Table 4: Moments, Moment Redistribution, Deflection and failure load.

Specimen	$R\ (kN)$	$Q\ (kN)$	$P_u\ (kN)$	Deflection (mm)	Exp. moment $(kN.m)$		Elastic moment $(kN.m)$		β_1 %	Mode of failure
					Hogging	Sagging	Hogging	Sagging		
BS1	23.80	71.2	190	11.00	24.68	25.14	33.26	19.32	25.78	shear
BS2	17.50	94	223	9.00	28.44	23.3	37.18	17	23.5	shear
BS3	13.60	122.4	272	8.90	30.00	18.95	38.2	12.25	21.46	shear

- $R\ (kN)$: End reaction.
- $Q\ (kN)$: Ultimate shear force at central support,
- $P_u\ (kN)$: Beam ultimate load,
- β_1 %: Experimentally determined moment redistribution ratio.

3.4. Summary of Experimental results

- Reducing the a/d ratio from 2.6 to 1.5 increased the shear capacity by 42%.
- All beams failed in shear, with critical cracking initiating near the middle support.
- Higher shear strength came at the cost of reduced ductility and redistribution.
- Moment redistribution improved with decreasing a/d ratio, but excessive reduction led to brittle failure.

4. Nonlinear finite element (FE) modeling

In the finite element simulations, concrete was represented using the eight-node SOLID65 element in ANSYS (Figure 5) [27]. This element can capture tensile cracking, compressive crushing, and plastic deformation in three orthogonal directions, making it appropriate for reinforced concrete modelling. Each node had three translational degrees of freedom in the global x, y, and z directions.

4.1. Material characteristics and element types

The constitutive behavior of concrete included both linear isotropic and multi-linear isotropic components, with nonlinear behavior described using the Willam–Warnke failure criterion [30]. Shear transfer coefficients were set to 0.3 for open cracks and 0.8 for closed cracks, following recommendations from previous studies [28]. The elastic modulus was calculated in accordance with ACI 318 [17]:

$$E_c = 4700\sqrt{f_c} \tag{6}$$

where f_c is the cylinder compressive strength in MPa. The modulus of rupture was determined as:

$$f_r = 0,62\sqrt{f_c} \tag{7}$$

In this study f_c and f_r were taken as 25 MPa and 3.10 MPa, respectively. Steel reinforcement was modelled using LINK180 elements (Figure 6) [27], which capture elastic–plastic behavior under axial loading. Material properties for both 16 mm high-yield deformed bars and 6–8 mm mild steel stirrups were obtained from tensile tests (Table 2). The stress–strain response was modelled as bilinear with zero tangent stiffness in the plastic range, and Poisson's ratio was set to 0.30. Loading and support plates were simulated using SOLID185 elements (Figure 7) [27], with an elastic modulus of 200 GPa and a Poisson's ratio of 0.30.

4.2. Model Structure

The reinforcement in the finite element model was represented using LINK180 elements, embedded directly within the SOLID65 concrete elements. A perfect bond was assumed between steel and surrounding concrete, meaning no slip or interface elements were introduced. Similarly, the SOLID185 steel bearing plates used at the loading and support points were modelled in full contact with the concrete to ensure complete load transfer.

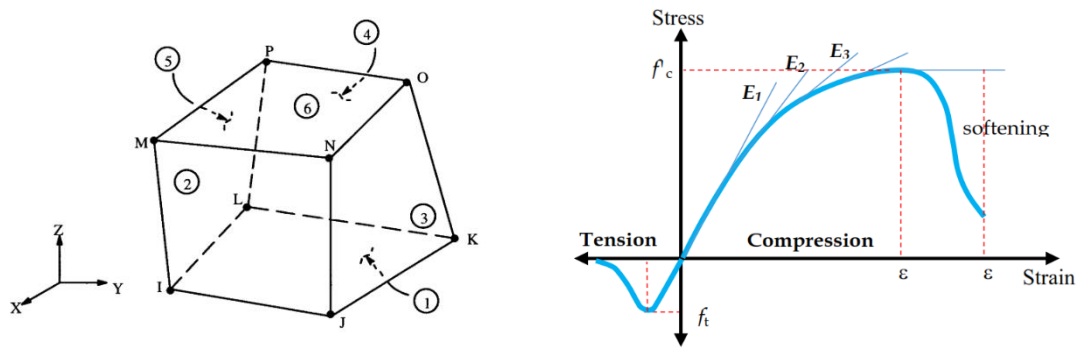

Fig. 4: SOLID65 geometry and stress-strain curve for concrete [27].

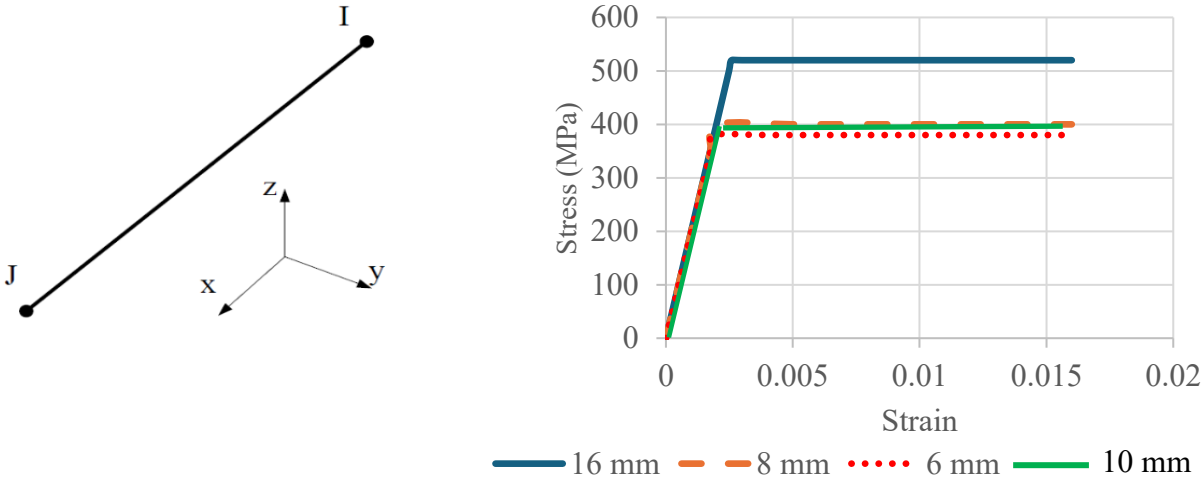

Fig. 5: LINK180 Geometry [27], and Stress-strain curve for steel bars.

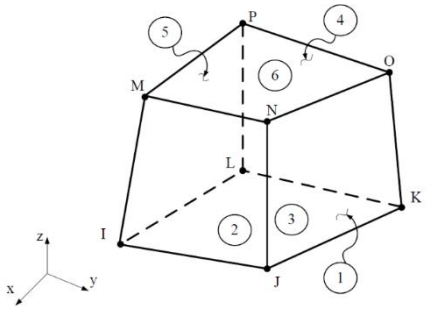

Fig. 6: SOLID185 Geometry [27].

The continuous beams tested in the laboratory exhibited symmetry both along their longitudinal axis through the central support and vertically through the centroidal axis of the cross-section. To reduce computational demand while maintaining modelling accuracy, only one-quarter of each beam was simulated (Figure 8a–c). Appropriate symmetry boundary conditions were applied to the cut planes to represent the remaining portions of the structure. Support conditions in the numerical model replicated those used experimentally (Figure 2). The central support was simulated as a hinged connection, restraining horizontal and vertical translation but allowing rotation, while the end support was modelled as a roller, restraining vertical movement only. No lateral restraints were applied, allowing free transverse deformation during loading. A mesh sensitivity analysis was conducted to determine an optimal element size that balances accuracy and computational cost. Mesh sizes from 75 mm

to 15 mm were examined. Coarser meshes resulted in premature numerical instability and reduced accuracy, whereas very fine meshes significantly increased the computational time. A final element size of 50 × 20 × 20 mm was selected, as it produced less than 0.05% variation in key response parameters compared to the finest tested mesh, while maintaining a reasonable solution time.

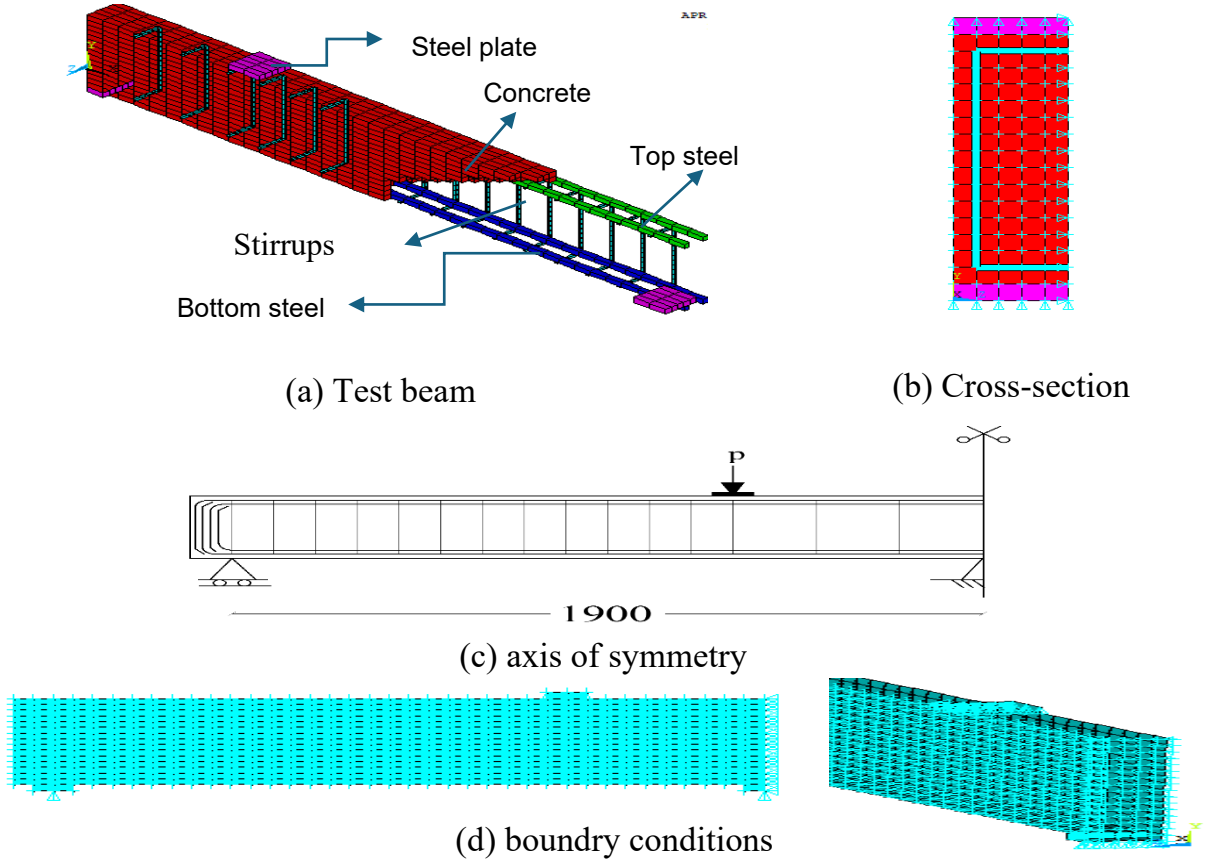

Fig. 8: (a) Geometry of the test beam, (b) Cross-section, (c) Axis of symmetry, and (d) Boundary conditions. Note: Lateral displacements were not restrained in the simulation to reflect the absence of lateral supports during experimental testing.

4.3. Numerical Solution Parameters

The nonlinear static analysis was carried out in incremental load steps to capture both the pre-cracking and post-cracking response of the beams. Each load step applied a fraction of the total load in the direction of the actuator, allowing the stiffness matrix to be updated progressively as material nonlinearity developed. The solution employed the Newton–Raphson iterative procedure, which repeatedly updates the structural stiffness until equilibrium is achieved within a specified tolerance at the end of each load step. This approach ensures stable convergence even when stiffness degradation occurs due to cracking and yielding. The analysis type was set to small-displacement static conditions, consistent with the experimental deformation levels. Convergence checks were based on both force and displacement criteria, with tolerances of 0.005 and 0.05, respectively. These limits were found to provide a balance between computational stability and accuracy in reproducing the experimental load–deflection behavior. All other solution controls, including time stepping

and contact status updates, were set to maintain stability without artificially constraining crack development or redistribution effects.

4.4. Model Verification

The finite element model developed in ANSYS was validated against the experimental results obtained for the three continuous RC beams (BS1, BS2, and BS3) tested under symmetrical four-point bending. Validation involved a direct comparison of load–deflection curves, moment redistribution trends, cracking patterns, and ultimate load capacities.

As shown in Table 5, the FEM-predicted yielding and ultimate loads were within approximately **3%** of the experimental values for all beams. The numerical load–deflection responses (Figure 9) reproduced the initial elastic stiffness, the gradual reduction in stiffness after cracking, the yield plateau, and the peak load with close agreement to the experimental curves. It is calculated by:

$$\boldsymbol{\beta = \frac{M_e - M_{ex}}{M_e} x100} \quad (8)$$

Figure 10 demonstrates that the FEM and experimental results followed similar trends at the middle support, with deviations not exceeding 20%, which is considered acceptable for nonlinear RC beam analysis.

The predicted cracking patterns and failure modes closely matched those observed in the laboratory. The FEM successfully identified the initiation of flexural cracks, the formation of diagonal shear cracks in high-shear regions, and the progression to the critical shear crack that led to failure (Figures 11–13). The orientation and location of major cracks were consistent with experimental observations, and the predicted failure mode was shear-dominated in all cases, as in the physical tests. This level of agreement in load response, redistribution behavior, and crack development confirms the robustness of the numerical model for simulating the structural performance of continuous RC beams. With this validation, the FEM was deemed suitable for the extended parametric study described in the following section.

Table 5: Comparison between the Experimental and FEM results at yield and ultimate loads.

Beam	Yielding load at hogging region (kN)			Ultimate load (kN)		
	Exp.	FEM	Exp./ FEM	Exp.	FEM	Exp./ FEM
BS1	180	185	0.97	190	199	0.96
BS2	200	208	0.96	223	230	0.97
BS3	239	251	0.95	272	275	0.99

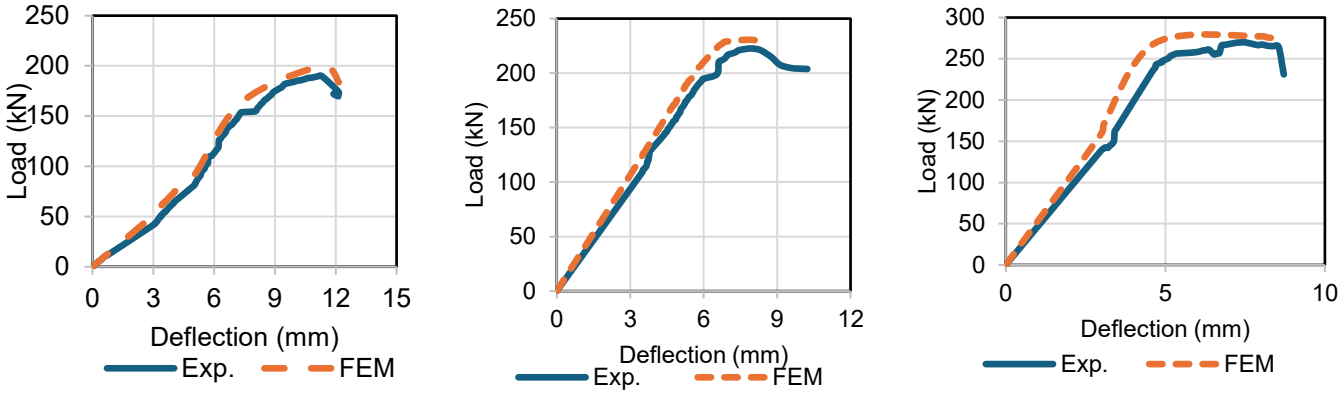

(a) BS1 (b) BS2 (c) BS3

Fig. 7: Load-deflection behavior of tested beams.

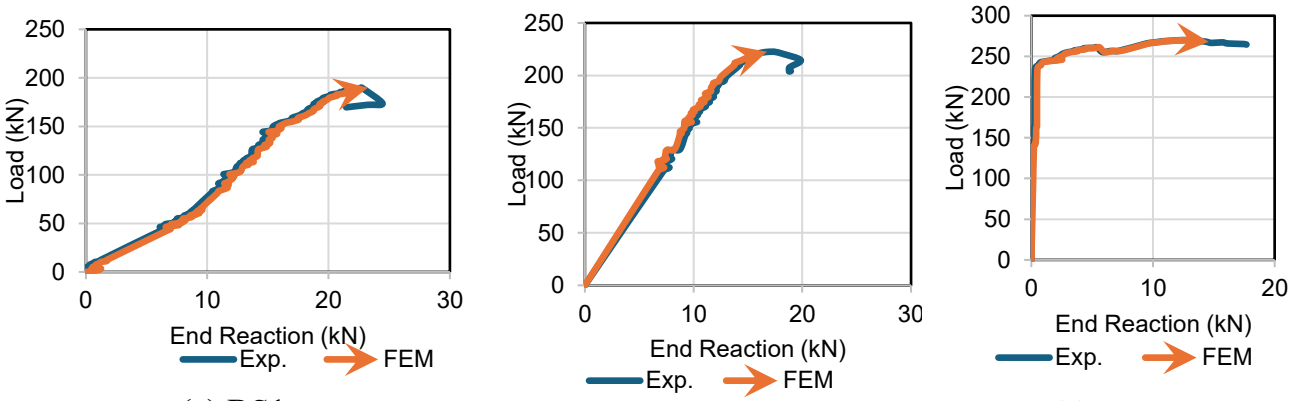

(a) BS1 (b) BS2 (c) BS3

Fig. 8: Load versus end reactions of tested beams.

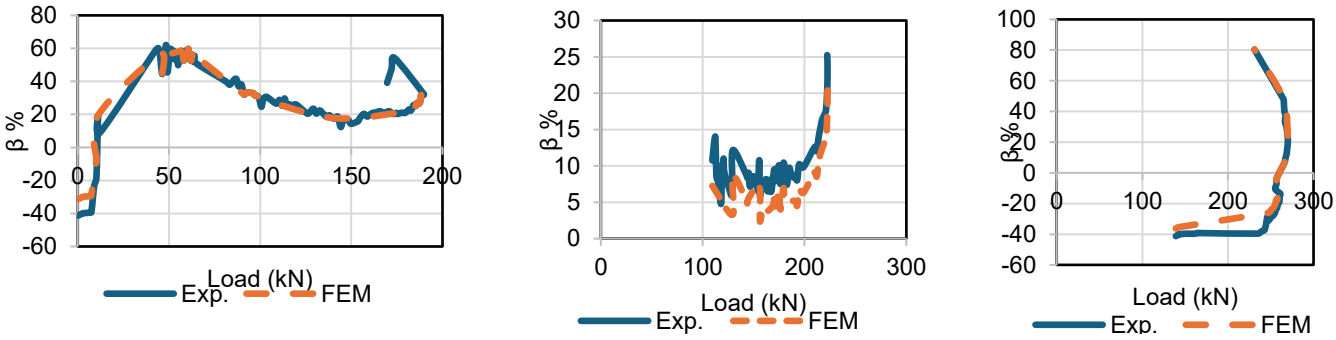

(a) BS1 (b) BS2 (c) BS3

Fig. 9: Load versus moment redistributions at the middle support of beams BS1, BS2 and BS3.

Fig. 10: Numerical crack propagation pattern of beam BS1 from FEM analysis, showing critical diagonal shear cracking.

Fig. 11: Numerical crack pattern for beam BS2 from FEM, capturing diagonal cracking consistent with experimental results.

4.5. Summary of Numerical simulation results

- The finite element (FE) models developed in ANSYS APDL closely replicated the experimental results of continuous RC beams, with ultimate load predictions within 3–5% of test values.
- The FE simulations successfully captured the load-deflection behavior, including:
  - Initial elastic stiffness
  - Post-cracking degradation
  - Yield plateau and peak strength
  - Brittle shear failure at ultimate loads
- The models effectively reproduced crack initiation and propagation, with predicted shear crack patterns and failure modes aligning well with experimental observations (Figures 11–13).
- Moment redistribution behavior was accurately simulated. The calculated redistribution ratios (β) at the critical middle support differed from experiments by no more than 20%, indicating acceptable accuracy for nonlinear structural response modelling.

5. Parametric Study

After validating the finite element model against the experimental program, a broader parametric investigation was carried out to quantify the influence of shear span-to-depth ratio (a/d), and transverse reinforcement ratio on the structural response of continuous RC beams. In total, 11 FE beam models were generated in ANSYS by systematically varying (a/d), and web reinforcement content, while maintaining all other geometric and material properties consistent with the experimental specimens. Specimen layouts, including reinforcement arrangements, are presented in Figure 14, with corresponding details listed in Table 6.

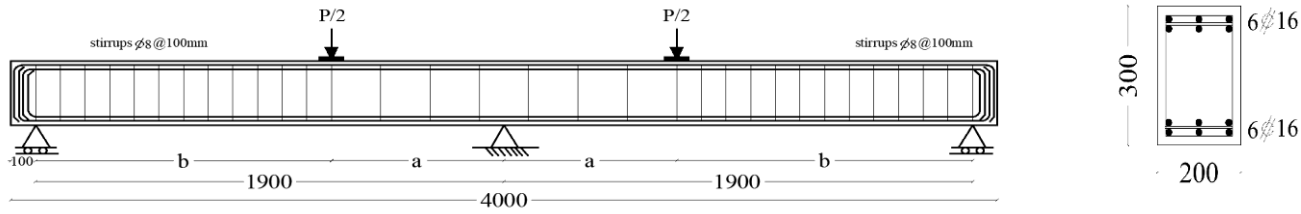

Fig. 14: Details of test specimens (all dimensions in mm).

6. General behavior, cracking pattern, and mode of failure

At various loading stages, all test beams exhibited identical cracking behavior until failure. All beams started to develop shear and flexural cracks as the load was gradually applied. The flexural cracks stopped forming at a specific load level, whereas further shear cracks began to emerge. All beams exhibited shear failure at ultimate load, and a critical shear crack line developed next to the centre support of the two-span continuous RC beams. Table 7 shows the shear failure loads for test beams. Failure occurred in all beams after the yielding of two adjacent stirrups in the internal shear span. Figure 15 clearly shows that beams reinforced with a high web reinforcement ratio have more shear cracks than beams reinforced with a low ratio. Furthermore, beams with a high shear span-to-depth ratio have more shear cracks than beams with a low ratio. Figure 16 shows the mode of failure for test beams.

Table 6: Details of beams

Specimen	a/d	$a\ (mm)$	$b\ (mm)$	Stirrups	μ_{st}	Main reinforcement		(f_c) (MPa)
						Top	Bottom	
C1	2	600	1300	5Φ6/m	0.280	6Φ16	6Φ16	26
C2	2	600	1300	7Φ6/m	0.373			
C3	2	600	1300	10Φ6/m	0.560			
C4	2	600	1300	5Φ8/m	0.500			
C5	1	300	1600	7Φ8/m	0.667			
C6	1.5	450	1450					
C7	1.7	500	1400					
C8	2	600	1300					
C9	2.5	750	1150					
C10	3	900	1000					
C11	1.7	500	1400	10Φ8/m	1.00			

Table 7: End reaction, shear force, Moments and Moment Redistribution at ultimate load

Specimen	R (kN)	Q (kN)	P_u^* (kN)	FEM moment, (kN. m)		Elastic moment (kN. m)		β_1 %	β_2%
				Hogging	Sagging	Hogging	Sagging		
C1	26	118	144	40	31.2	47.8	25.9	16	-20
C2	28.5	130	158.5	43.8	34.2	54	28.5	17	-20
C3	31.6	145.4	177	49.3	37.9	58.9	31.7	16.3	-19.5
C4	30.25	143	173.25	49.5	36.3	57.7	31.2	14.2	-16
C5	17.3	300	317.3	64	26	73	19	12	-37
C6	25	205	230	58.5	33.75	67.9	27.6	13.78	-22
C7	28	188	216	57.6	36.1	67.8	30.24	15.07	-19.4
C8	35.0	162.4	196.8	55.0	41.3	65.5	35.4	16	-16.7
C9	52.6	149.6	202.2	57	55.2	70	47.5	18.5	-16.2
C10	66.8	124	192.4	52.9	60.1	64.9	53.9	20	-11.5
C11	39	265	304	81.8	50.3	95.5	42.6	14.3	-18

R: End reaction, Q: Shear force, $P_u^* = \left(\frac{P_u}{2}\right)$: Ultimate load of one span, β_1: Moment redistribution ratio of hogging moment, β_2: Moment redistribution ratio of sagging moment.

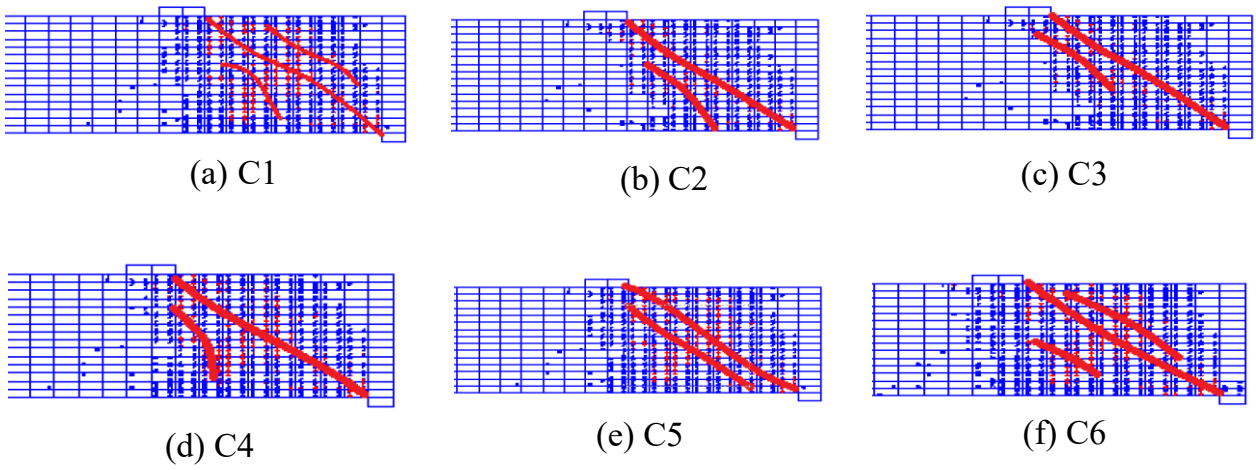

Fig. 15: Crack patterns and failure modes for beams C1–C6, illustrating effects of web reinforcement and a/d ratio on shear cracking.

7. Load-Deflection Response

Figures 16 and 17 illustrate the relationship between the applied load for one span (P_u^*) and point load deflection for all tested beams. In general, the beams exhibited linear load-deflection behavior with a steep slope in the uncracked stage at the start of the loading. Following cracking, the flexural stiffness decreased as the load increased; the flexural stiffness and deflection are dependent on the axial stiffness of the reinforcing bars [33]. Figure 16 shows the effect of the percentage of web reinforcement on the ultimate load. Comparing the diagrams, it can be observed that the influence of varying the web reinforcement ratio while keeping the shear span-to-depth ratio constant at a/d = 2. The beams with higher web reinforcement ratios (C3, C4 and C8) exhibit improved load-carrying capacity and slightly higher stiffness compared to the beams with lower web reinforcement ratio (C1 and C2). However, the differences in the load-deflection response are not very pronounced between these beams. This observation suggests that for the shear span-to-depth ratio of a/d = 2, increasing the web reinforcement ratio beyond a certain point may not significantly enhance the overall load-deflection behavior or shear strength. The presence of minimum web reinforcement (as in C1) appears to be sufficient to ensure reasonable performance up to the ultimate load stage for this relatively low a/d ratio. It is important to note that these comparisons are specific to the a/d = 2 case, and the influence of web reinforcement ratio may be more pronounced for higher shear span-to-depth ratios, where shear stresses become more critical. Generally, as designed, the ultimate capacity of beams (C2, C3, C4, and C8) is increased compared with the control beam C1 by (10, 23, 20, 36%) respectively. This is due to the fact that increasing the amount of web reinforcement by decreasing the spacing between stirrups increases the shear strength of the beam carried by concrete and stirrups. The ultimate load of concrete beams decreases with limited values as the (a/d) ratio increases. The measured deflection of beams with high (a/d) ratios was consistently lower than that of beams with low (a/d) ratios at any load level. Beam C5 has stiffness higher than other beams, as shown in Figure 17.

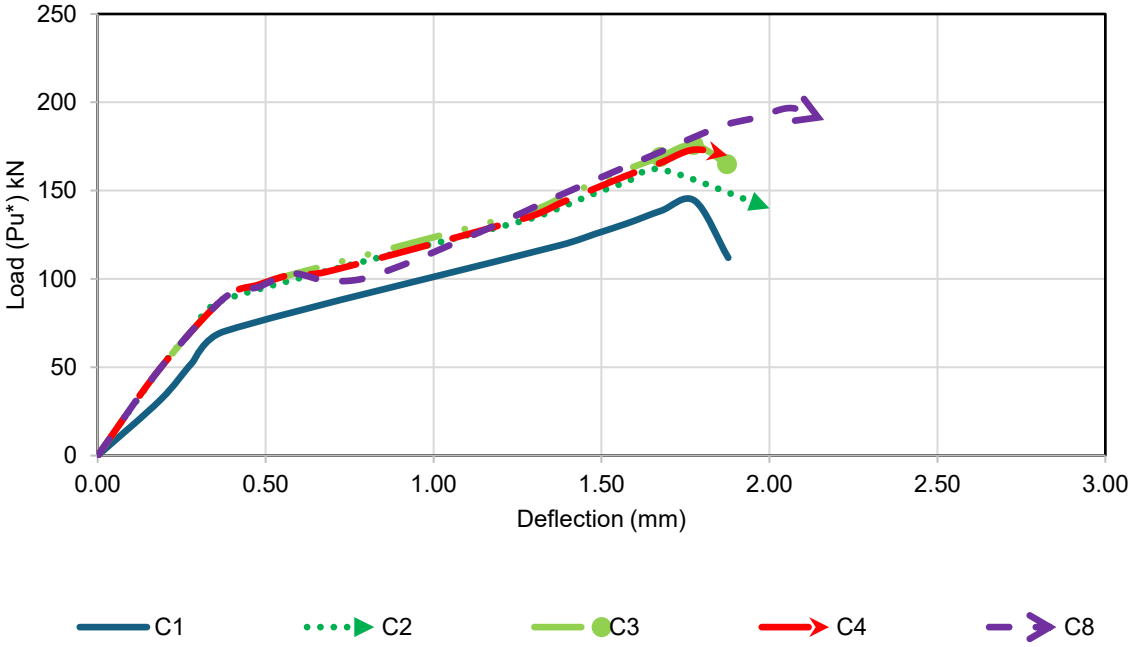

Fig. 126: Load-deflection relationship at load point of test beams.

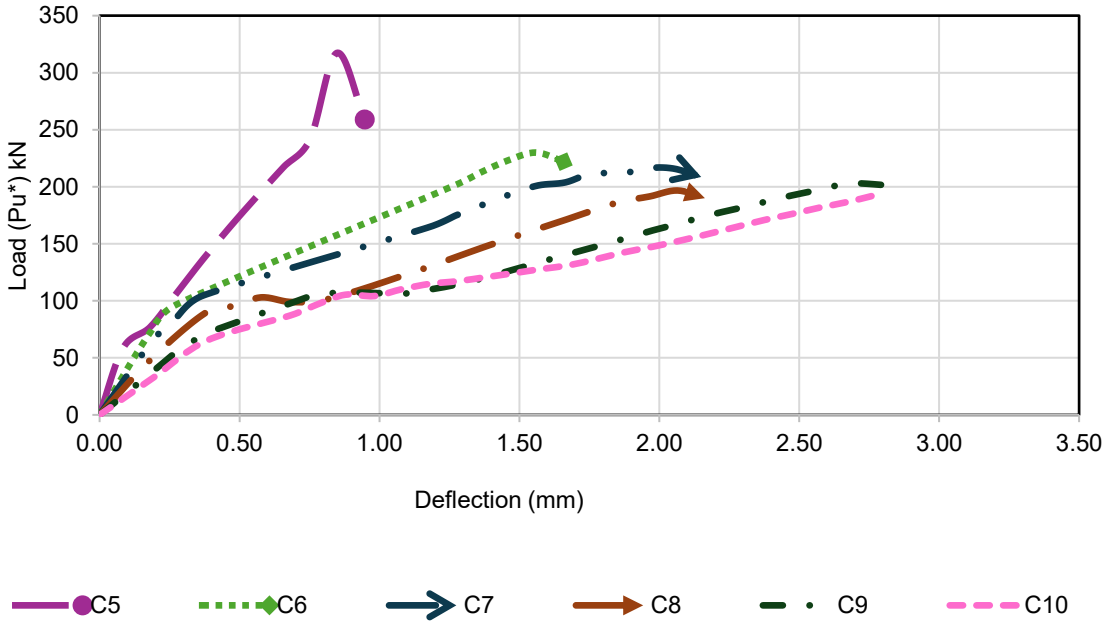

Fig. 137: Effect of (a/d)ratio on Load-deflection relationship of test beams.

8. Moment Redistribution

The evolution of the moment redistribution ratio (β) for all specimens is plotted in Figure 18 and numerically summarized in Table 7. This parameter was evaluated by comparing the bending moments at the middle support (hogging region) and at mid-span (sagging region) throughout the entire loading process, from the initial application of load up to failure. At the early stages, before cracking occurred in the hogging zone, the redistribution ratio (β) assumed negative values. This indicates that the experimentally measured moment in the

hogging region exceeded the corresponding elastic moment, implying a transfer of internal forces from the sagging span toward the support region. Once the first flexural cracks developed at the support, β progressively decreased and approached zero at the cracking load. Beyond this stage, the redistribution mechanism reversed: internal forces shifted from the negative moment zone toward the positive span regions. Between cracking and yielding, the redistribution ratio increased gradually, while after yielding it rose more sharply, reaching peak values near failure. The role of shear reinforcement was found to be relatively limited. For instance, beam C1, with the lowest web reinforcement ratio, exhibited redistribution values of approximately 14% at yield and 16% at failure. In comparison, beam C11, containing the highest stirrup ratio, showed a reduction in redistribution capacity, with average values of 21% at yield and 11% at failure, relative to beam C1. This suggests that variations in shear reinforcement ratio exert only a secondary influence on redistribution behavior. By contrast, the shear span-to-depth ratio (a/d) had a pronounced effect. Beams C5–C10, which share the same stirrup ratio but differ in a/d, clearly demonstrate this trend. Beam C5, with the lowest (a/d), exhibited a redistribution ratio of about 12%, whereas beam C10, with the highest (a/d)), showed a value nearly 67% greater than that of C5 (see Table 7). This confirms that a/d is a dominant parameter controlling redistribution, as shorter spans favor shear resistance but reduce ductility, while larger spans enhance the capacity for moment transfer between critical regions. Overall, Table 7 compiles the shear forces, support reactions, ultimate loads, hogging/sagging moments, and redistribution ratios, while Figure 18 provides a consolidated visual of how β evolves with load level and varies with reinforcement and a/d. The results establish $(\frac{a}{d})$ as the dominant parameter governing redistribution, with transverse reinforcement acting mainly as a modifier rather than a driver.

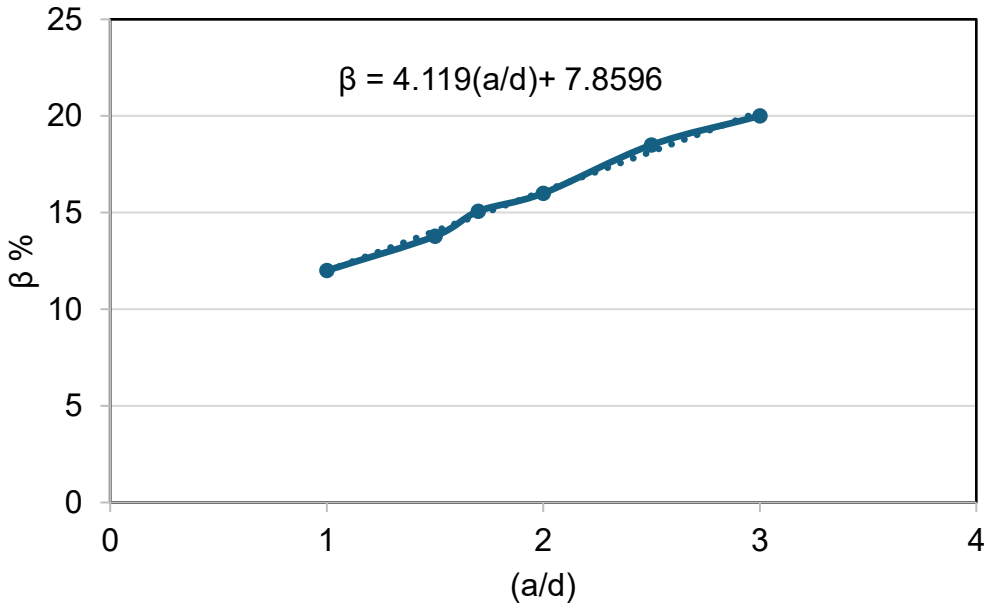

Fig. 1814: Variation in moment redistribution ratio (β) with changes in shear span-to-depth ratio (a/d) for all tested beams.

9. Development of Design Equations Using Elastic Moments and Redistribution Ratios

Although many design codes employ linear elastic analysis for continuous reinforced concrete (RC) beams, experimental and analytical studies [31–34] consistently show that such members undergo significant moment redistribution prior to failure. The extent of redistribution permissible in design is often capped by simplified limits that do not explicitly account for key influencing parameters, which can lead to either unnecessarily conservative or unsafe predictions of structural capacity and serviceability. ACI 318 [17] limits $\boldsymbol{\beta}$ based on the net tensile strain in the extreme tension reinforcement, with a maximum allowance of 20%.

$$\boldsymbol{\beta}\% \leq \mathbf{1000}\ \varepsilon_t \tag{9}$$

The negative moment determined by an elastic analysis can be changed by a factor according to the CSA code [33] with a maximum of 20%.

$$\boldsymbol{\beta}\% \leq \mathbf{30 - 50}\ (\frac{c}{d}) \tag{10}$$

Where $(\frac{c}{d})$ is the ratio of a cross section's neutral axis depth to its effective depth at the ultimate limit state. In Europe, EC2 [20] and MC10 [34] also determine the degree of moment redistribution using the parameter $(\frac{c}{d})$:

$$\boldsymbol{\beta}\% \leq \mathbf{0,56 - 1,25}\ (\mathbf{0,6} + \frac{\mathbf{0,0014}}{\varepsilon_u})\frac{c}{d} \quad \text{for } \boldsymbol{f_{ck} \leq 50MPa} \tag{11}$$

$$\boldsymbol{\beta}\% \leq \mathbf{0,46 - 1,25}\ (\mathbf{0,6} + \frac{\mathbf{0,0014}}{\varepsilon_u})\frac{c}{d} \qquad \textbf{for } \boldsymbol{f_{ck} > 50MPa} \tag{12}$$

with a limit of 20% for low-ductility steel and 30% for high- and normal-ductility steel. (ε_u) denotes the ultimate concrete compressive strain, and $(\boldsymbol{f_{ck}})$ is the concrete cylinder compressive strength. According to the British standard [19], the degree of moment redistribution is estimated using the neutral axis depth (c) of the cross section, and the moments can be redistributed using an elastic analysis.

$$\boldsymbol{\beta}\% \leq (\mathbf{60 - 100}\ \frac{c}{d}) \tag{13}$$

Tarek et al. [7] also determined the moment redistribution ratio of normal strength RC beams, which takes the longitudinal reinforcement ratio into account as mentioned in Eq. 14:

$$\boldsymbol{\beta = 32.763 \ln \frac{A_{ss}}{A_{sh}} + 5.0611 \ln(\rho_s - \rho_{smin}) + 13.6988} \tag{14}$$

Table 6 reveals that for all specimens, the outcomes of the design codes previously discussed provide inconsistent outcomes and differ noticeably from those of the FE analysis. Tarek et

al. equation [7] is determined to be the results' closest approximation; however, the equivalent values are constant and unaffected by changes in $(\frac{a}{d})$. As a result, it is shown using Figure 10 as a logarithmic function that the values of the redistribution of moments are significantly influenced by the values of $(\frac{a}{d})$. As a result, the Tarek equation [7] was developed in this study by incorporating the effect of the shear span to depth ratio $(\frac{a}{d})$.

For one concentrated load:

$$\boldsymbol{\beta = 32.763 \ln(\frac{A_{ss}}{A_{sh}}) + 5.0611 \ln(\rho_s - \rho_{smin}) + 6.46 \ln\left(\frac{a}{d}\right) + 7.66} \quad (15)$$

For two concentrated loads:

$$\boldsymbol{\beta = 32.763 \ln(\frac{A_{ss}}{A_{sh}}) + 5.0611 \ln(\rho_s - \rho_{smin}) + 6.46 \ln\left(\frac{a}{d}\right)_1 + 6.46 \ln\left(\frac{a}{d}\right)_2 + 7.66} \quad (16)$$

Tables 8–10 compare the proposed equations with FEA results and code-based predictions. Across the full specimen set, the mean ratio of predicted to FEA $\boldsymbol{\beta}$ values are 0.96, with an average deviation below 5%. The model performs most accurately for beams with ($1.5 \leq a/d \leq 2.5$), which covers most practical design cases.

For very low a/d values (e.g., specimen C5, a/d = 1.0), the model slightly underestimates $\boldsymbol{\beta}$, likely due to shear-dominated response and reduced plastic rotation capacity. For high a/d ratios (e.g., C10, a/d = 3.0), minor overprediction occurs, potentially because of increased flexural influence not fully captured in the simplified form.

Compared with existing provisions, which either fix redistribution caps or neglect a/d effects, the proposed equation provides a more adaptable and accurate tool. Its explicit incorporation of a/d enables reliable application to short-span and deep beams, where conventional formulas may become overly conservative or unconservative.

Table 8: The comparison of the FEM results and the obtained equations at the hogging zone.

Specimen	Predicted	FEM	FEM/Predicted
C1	15.43	16	0.96
C2	15.43	17	0.91
C3	15.43	16.3	0.95
C4	15.43	14.2	1.09
C5	10.95	12	0.91
C6	13.57	13.78	0.98
C7	14.38	15.07	0.95
C8	15.43	14.3	1.08
C9	16.87	18.5	0.91
C10	18.05	20	0.90
C11	14.38	14.3	1.01

Table 9: Results of FEM in terms of moment redistribution.

Specimen	ε_t	ε_u	c/d	β %						
				ACI	CAS	EC2	BSI	Tarek	Predicted	FEM
C1	0.100	0.098	0.185	1.00	20.75	9.09	41.50	16.99	15.43	16.00
C2	0.080	0.117	0.203	0.80	19.85	10.41	39.70	16.99	15.43	17.00
C3	0.103	0.098	0.186	1.03	20.70	8.84	41.40	16.99	15.43	16.30
C4	0.090	0.102	0.196	0.90	20.20	7.67	40.40	16.99	15.43	14.20
C5	0.075	0.116	0.201	0.75	19.95	10.60	39.90	16.99	10.95	12.00
C6	0.080	0.121	0.222	0.80	18.90	7.24	37.80	16.99	13.57	13.78
C7	0.098	0.047	0.167	0.98	21.65	18.71	43.30	16.99	14.38	15.07
C8	0.093	0.102	0.197	0.93	20.15	7.43	40.30	16.99	15.43	14.30
C9	0.115	0.106	0.200	1.15	20.00	7.98	40.00	16.99	16.87	18.50
C10	0.153	0.120	0.222	1.53	18.90	6.98	37.80	16.99	18.05	20.00
C11	0.100	0.115	0.200	1.00	20.00	10.57	40.00	16.99	14.38	14.30

Table 10: Experimental and predicted moment redistribution ratios of the continuous reinforced concrete beams

Reference	Beam	$(a/d)_1$	$(a/d)_2$	$A_{ss}(mm^2)$	$A_{sh}\ (mm^2)$	$b\ (mm)$	$d\ (mm)$	ρ_s	ρ_{smin}	$\beta_{exp.}$	$\beta_{pre.}$
N. Baša [35]	S1-15	4.2	---	304	270	150	220	0.921	0.306	15.0	18.36
S.M. Hasanur Rahman [23]	SuR-II	5.2	---	850	500	700	270	0.450	0.306	25.0	25.89
AbdulAziz Abdul Samad [16]	(Beam 3-0)	3.3	4.8	600	1200	150	325	1.231	0.306	2.3	2.40
Khalifa, A.Tumialan [36]	CW1	4	---	1600	1600	150	265	4.025	0.239	25.0	23.35
	CO1	4	----	1600	1600	150	265	4.025	0.239	25.0	23.35

10. Prediction of ultimate load

The shear capacity of RC continuous beams with shear reinforcement is essentially equal to the sum of the concrete (V_c) and stirrup contributions (V_s) . Shear force for continuous RC beam at the middle support is obtained by (Q):

$$\boldsymbol{Q = V_n\, , b\, , d} \tag{17}$$

To determine the total ultimate shear load for one span of a continuous concrete beam and the reaction of the edge support. First, the elastic bending moment and the moment redistribution ratio are used to determine the final bending moment value at the middle support. The elastic bending moments at mid-span and over the middle support of the two span beams have various shear spans indicated in [39], where P and L are the mid-span applied load and beam span, respectively, as shown in Figure 19.

$$M_B = \frac{P,a,b}{L^3}(L + a)L \tag{18}$$

$$M_C = \frac{P,a}{2}\left(2 - 3\frac{a}{L} + \frac{a^3}{L^3}\right) \tag{19}$$

$$M_{B\,Final} = M_B(1 - \beta) \tag{20}$$

$$P = \frac{Q,L - M_B\,Final}{a} \tag{21}$$

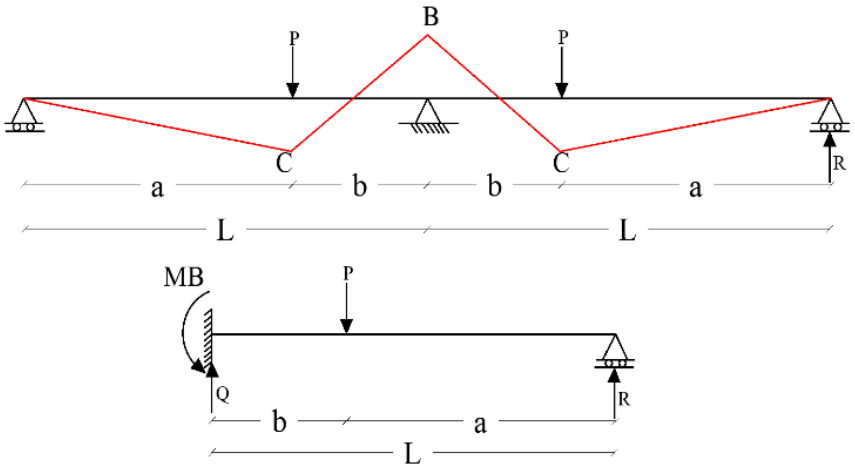

Fig. 19: Elastic bending moment distribution with constant flexural stiffness.

11. Conclusions

This study presented a combined experimental–numerical investigation into the shear strength and moment redistribution behavior of continuous RC beams, focusing on the influence of shear span-to-depth ratio (a/d) and transverse reinforcement ratio. The main findings are:

1. Reducing a/d from 2.6 to 1.5 increased shear capacity by up to 42%, but reduced ductility and redistribution potential.
2. Increasing transverse reinforcement enhanced shear resistance but had minimal effect on redistribution, which was governed primarily by a/d.
3. A new empirical equation was developed to predict moment redistribution ratios incorporating a/d, achieving prediction errors within ±5% of FEM and experimental results, and outperforming existing code expressions.
4. The validated FEM model reliably captured load–deflection behavior, cracking patterns, and redistribution trends, supporting its use in advanced structural analysis.

These results provide a rational framework for linking shear strength and redistribution limits, offering direct implications for refining shear design provisions in major structural codes. Adoption of the proposed model can improve the accuracy and reliability of designs for continuous RC beams, especially in cases involving short-span or deep-section members.

References

[1] R. Krishnan and V. Lakshmi Sivakumar, "Profound Impact of Shear Wall on Stability of Regular and Irregular Reinforced Concrete Structures – A Review," Mater Today Proc, May 2023, Doi: 10.1016/J.MATPR.2023.05.130.

[2] S. A. Kristiawan, H. A. Saifullah, and A. Supriyadi, "Influence of patching on the shear failure of reinforced concrete beam without stirrup," Infrastructures (Basel), vol. 6, no. 7, Sep. 2021, Doi: 10.3390/infrastructures6070097.

[3] R. Malm, "Shear cracks in concrete structures subjected to in-plane stresses," 2006.

[4] G. L. Golewski, "The Phenomenon of Cracking in Cement Concretes and Reinforced Concrete Structures: The Mechanism of Cracks Formation, Causes of Their Initiation, Types and Places of Occurrence, and Methods of Detection—A Review," Buildings, vol. 13, no. 3. MDPI, Mar. 01, 2023. Doi: 10.3390/buildings13030765.

[5] A. Saribiyik, B. Abodan, and M. T. Balci, "Experimental study on shear strengthening of RC beams with basalt FRP strips using different wrapping methods," Engineering Science and Technology, an International Journal, vol. 24, no. 1, pp. 192–204, Feb. 2021, Doi: 10.1016/j.jestch.2020.06.003.

[6] A. Shomali, D. Mostofinejad, and M. R. Esfahani, "Shear strengthening of RC beams using EBRIG CFRP strips: a comparative study," European Journal of Environmental and Civil Engineering, vol. 25, no. 14, pp. 2540–2556, 2021, Doi: 10.1080/19648189.2019.1633413.

[7] T. Abdelaleem, H. M. Diab, and M. M. M. Rashwan, "New aspects about the effect of critical regions reinforcement on the strength and moment redistribution of RC continuous T-beams (Experimental and numerical study)," Structures, vol. 34, pp. 4834–4850, Dec. 2021, Doi: 10.1016/j.istruc.2021.10.065.

[8] H. M. A. Diab, T. Abdelaleem, and M. M. M. Rashwan, "Moment redistribution and flexural performance of RC continuous T-beams strengthened with NSM FRP or steel bars," Structures, vol. 28, pp. 1516–1538, Dec. 2020, Doi: 10.1016/j.istruc.2020.09.003.

[9] A. Goh and Walraven, "Shear Friction Along Continuous Concrete Beams," Heron, vol. 52, no. 1, 2007.

[10] K. Yang, "Shear Strength Prediction of Reinforced Concrete Continuous Beams," 2007.

[11] C. Broms, "Elasticity, Plasticity and Shear in Reinforced Concrete Beams and Frames," Royal Institute of Technology, 2000.

[12] J. Kuang and C. Morley, "Simplified Equation for Enhanced Shear Strength of Continuous Beams," 1993.

[13] T. Roberts and Moreno, "Shear Strength of Continuous Reinforced Concrete Beams," 1976.

[14] K. Tan and Et Al, "Shear Strength of Continuous Prestressed Concrete Beams," Magazine of Concrete Research, vol. 49, no. 179, 1997.

[15] S. Hwang, "Shear Strength Prediction for Discontinuous Prestressed Concrete Beams," 2000.

[16] A. F. Ashour and F. R. Tureyen, "Concrete shear strength: Test results and design equations," *ACI Structural Journal*, vol. 100, no. 5, pp. 612–619, 2003.

[17] Building Code Requirements for Structural Concrete (ACI 318-19) Commentary on Building Code Requirements for Structural Concrete (ACI 318R-19). 2019.

[18] "British Standards Institution. Structural use of concrete," Part 1. BS 8110, 1995.

[19] British Standards Institution (BSI), "Brussels: European Committee for Standardization," BS8110, London, UK; (2007), 2007.

[20] European Committee for Standardization., "Eurocode 2: design of concrete structures– Part 1-1: general rules and rules for buildings. DS/EN 1992-1-1 + AC," Brussels: European Committee for Standardization, 2009.

[21] K. Mahmoud and E. El-Salakawy, "Effect of Transverse Reinforcement Ratio on the Shear Strength of GFRP-RC Continuous Beams," 2015, Doi: 10.1061/(ASCE)CC.1943-5614.

[22] A. Monserrat López, P. F. Miguel Sosa, J. L. Bonet Senach, and M. Á. Fernández Prada, "Experimental study of shear strength in continuous reinforced concrete beams with and without shear reinforcement," Eng Struct, vol. 220, Oct. 2020, Doi: 10.1016/j.engstruct.2020.110967.

[23] S. M. H. Rahman, K. Mahmoud, and E. El-Salakawy, "Moment redistribution in glass fiber reinforced polymer-reinforced concrete continuous beams subjected to unsymmetrical loading," Eng Struct, vol. 150, pp. 562–572, Nov. 2017, Doi: 10.1016/j.engstruct.2017.07.066.

[24] A. Monserrat López, P. F. Miguel Sosa, J. L. Bonet Senach, and M. Á. Fernández Prada, "Influence of the plastic hinge rotations on shear strength in continuous reinforced concrete beams with shear reinforcement," Eng Struct, vol. 207, Mar. 2020, Doi: 10.1016/j.engstruct.2020.110242.

[25] A. Monserrat López, M. Fernánez Ruiz, and P. F. Miguel Sosa, "The influence of transverse reinforcement and yielding of flexural reinforcement on the shear-transfer actions of RC members," Eng Struct, vol. 234, May 2021, Doi: 10.1016/j.engstruct.2021.111949.

[26] A. Monserrat López and P. Miguel Sosa, "The influence of flexural reinforcement yielding on the shear strength of reinforced concrete beams with and without shear reinforcement," Hormigón y Acero, Nov. 2022, Doi: 10.33586/hya.2022.3087.

[27] **ANSYS, Inc. (2019).** *ANSYS Mechanical APDL Documentation, Release 19.0.* Canonsburg, PA, USA: ANSYS, Inc. Available at: https://www.ansys.com.

[28] N. Elmezaini and M. Ashour, "Nonlinear Analysis of Concrete Beams Strengthened with Steel Fiber-Reinforced Concrete Layer," 2015.

[29] R. von Mises, "Mechanik der festen Körper im plastisch- deformablen Zustand," Nachrichten von der Gesellschaft der Wissenschaften zu Göttingen, vol. 1, pp. 582–592, 1913.

[30] G. Benipal, A. K. Singh, R. Raveendra Babu, G. S. Benipal, and A. K. Singh, "Constitutive modeling of concrete: An overview CONSTITUTIVE MODELLING OF CONCRETE: AN OVERVIEW," 2005. [Online]. Available: https://www.researchgate.net/publication/228361687

[31] Cohn MZ, "Continuity in prestressed concrete partial prestressing. Partial prestressing, from theory to practice," Survey Reports, NATO ASI Series. Boston, Mass.: Martinus Nijhoff, vol. 1, pp. 189–256, 1986.

[32] CSA (Canadian Standard Association), "Code for the design of concrete structures for buildings. CSA/A23.3-14," Toronto, Ontario, Canada, 2014.

[33] FIB, "Survey Reports, NATO ASI Series. Boston, Mass.: Martinus Nijhoff," International Federation for Structural Concrete, Lausanne, Switzerland, 2012.

[34] https://www.pci.org/PCI/Publications/PCI_Journal/Issues/1988/March, "April/Prediction of the Load Capacity of Two Span Continuous Prestressed Concrete Beams," 1988.

[35] N. Baša, M. Ulićević, and R. Zejak, "Experimental research of continuous concrete beams with GFRP reinforcement," Advances in Civil Engineering, vol. 2018, 2018, Doi: 10.1155/2018/6532723.

[36] A. Khalifa, G. Tumialan, A. Nanni, and A. Belarbi, "Shear Strengthening of Continuous RC Beams Using Externally Bonded CFRP Sheets," American Concrete Institute, 1999.